RSC Advances

PAPER

View Article Online
View Journal | View Issue

Cite this: *RSC Adv.*, 2024, **14**, 19539

From waste to wealth: iron oxide doped hydroxyapatite-based biosensor for the colorimetric detection of ascorbic acid

Amir Badshah,[a] Sadaf Noreen,[a] Mohibullah Shah,[b] Muhammad Asad,[a] Riaz Ullah,[c] Essam A. Ali,[d] Jibran Iqbal,[e] Wei Sun*[f] and Umar Nishan *[a]

Ascorbic acid plays a pivotal role in the human body. It maintains the robustness, enlargement, and elasticity of the collagen triple helix. However, the abnormal concentration of ascorbic acid causes various diseases, such as scurvy, cardiovascular diseases, gingival bleeding, urinary stones, diarrhea, stomach convulsions, *etc.* In the present work, an iron-doped hydroxyapatite (HAp@Fe_2O_3)-based biosensor was developed for the colorimetric detection of ascorbic acid based on a low-cost, biocompatible, and ubiquitous material. Due to the catalytic nature of HAp owing to the acidic and basic moieties within the structure, it was used as a template for HAp@Fe_2O_3 synthesis. This approach provides an active as well as large surface area for the sensing of ascorbic acid. The synthesized platform was characterized by various techniques, such as UV-Vis, FTIR, SEM, XRD, TGA, EDX, *etc.* The HAp@Fe_2O_3 demonstrated inherent peroxidase-like activity in the presence of 3,3′,5,5′-tetramethylbenzidine (TMB) oxidized with the assistance of H_2O_2. It resulted in the color changing to blue-green, and after the addition of ascorbic acid, the color changed to colorless, resulting in the reduction of TMB. To achieve optimal sensing parameters, experimental conditions were optimized. The quantity of HAp@Fe_2O_3, H_2O_2, pH, TMB, time, and the concentration of ascorbic acid were fine-tuned. The linear range for the proposed sensor was 0.6–56 μM, along with a limit of detection of 0.16 μM and a limit of quantification of 0.53 μM. The proposed sensor detects ascorbic acid within 75 seconds at room temperature. The proposed platform was also applied to quantitatively check the concentration of ascorbic acid in a physiological solution.

Received 24th March 2024
Accepted 14th June 2024

DOI: 10.1039/d4ra02264e

rsc.li/rsc-advances

1 Introduction

Ascorbic acid (AA), also known as vitamin C, plays an important role in various redox metabolic reactions in the human body. As an efficient antioxidant, it helps in scavenging free radicals in the body to protect the cells from oxidative damage, enhance immunity, prevent scurvy, the common cold, cancer, *etc.* Its main source is fruits and vegetables, and it cannot be synthesized in the human body.[1] It is highly desirable to develop a robust, low-cost, and reliable platform for the sensing and monitoring of AA.

Various techniques have been used for the detection of ascorbic acid, such as electrochemical techniques,[2] fluorometric methods,[3] high-performance liquid chromatography, *etc.*[4] These techniques, despite their merits, have some drawbacks, such as complicated sample preparation steps that are time-consuming, costly, and require highly sophisticated instrumentation. These techniques require highly skilled operators, and acquiring and sustaining them in laboratories with limited resources is a big challenge. On the other hand, the colorimetric method has great potential for ascorbic acid detection owing to its simplicity, rapid operation, and cost-effectiveness.[5] The added advantage associated with this approach is that its results can be visualized by the unaided eye.[6]

Hydroxyapatite (HAp) holds a prime position among biomaterials and has been utilized for bone implants. HAp comprises the major component of bone mineral and is expressed through the chemical formula $Ca_{10}(PO_4)_6(OH)$.[7] HAp has been produced utilizing a variety of precursors as well as extracted from natural sources. The most common natural sources of HAp extraction are marine organisms, animals, algae, and minerals.[8] For the extraction of HAp, both marine and terrestrial animal bones, scales, and shells have been employed. Similarly, fruit peels, wood, flowers, leaves, and stalks, are considered other suitable sources of HAp.[9] In the present work, we have used waste chicken bones as a precursor for HAp extraction. Chicken is a highly consumed product worldwide, and it is estimated that its consumption generates around 68 billion tons of waste annually.

[a]*Department of Chemistry, Kohat University of Science and Technology, Kohat 26000, KP, Pakistan. E-mail: umarnishan85@gmail.com*

[b]*Department of Biochemistry, Bahauddin Zakariya University, Multan 66000, Pakistan*

[c]*Department of Pharmacognosy, College of Pharmacy, King Saud University Riyadh, Saudi Arabia*

[d]*Department of Pharmaceutical Chemistry, College of Pharmacy, King Saud University Riyadh, Saudi Arabia*

[e]*College of Interdisciplinary Studies, Zayed University, Abu Dhabi, 144534, United Arab Emirates*

[f]*Hainan International Joint Research Center of Marine Advanced Photoelectric Functional Materials, College of Chemistry and Chemical Engineering, Hainan Normal University, Haikou 571158, P. R. China. E-mail: sunwei@hainnu.edu.cn*

This enormous amount of waste needs to be used in a beneficial manner.[10] The extraction of HAp and fabrication of the colorimetric sensor reported in this work are an attempt to sustainably and beneficially use chicken waste. Various techniques have been reported to isolate HAp from waste materials, such as mechanochemical,[11] wet chemical methods, *etc.*[12] However, the above-mentioned methods are laborious and require sophisticated equipment and apparatus. Therefore, in the present work, the calcination method has been used for the preparation of HAp

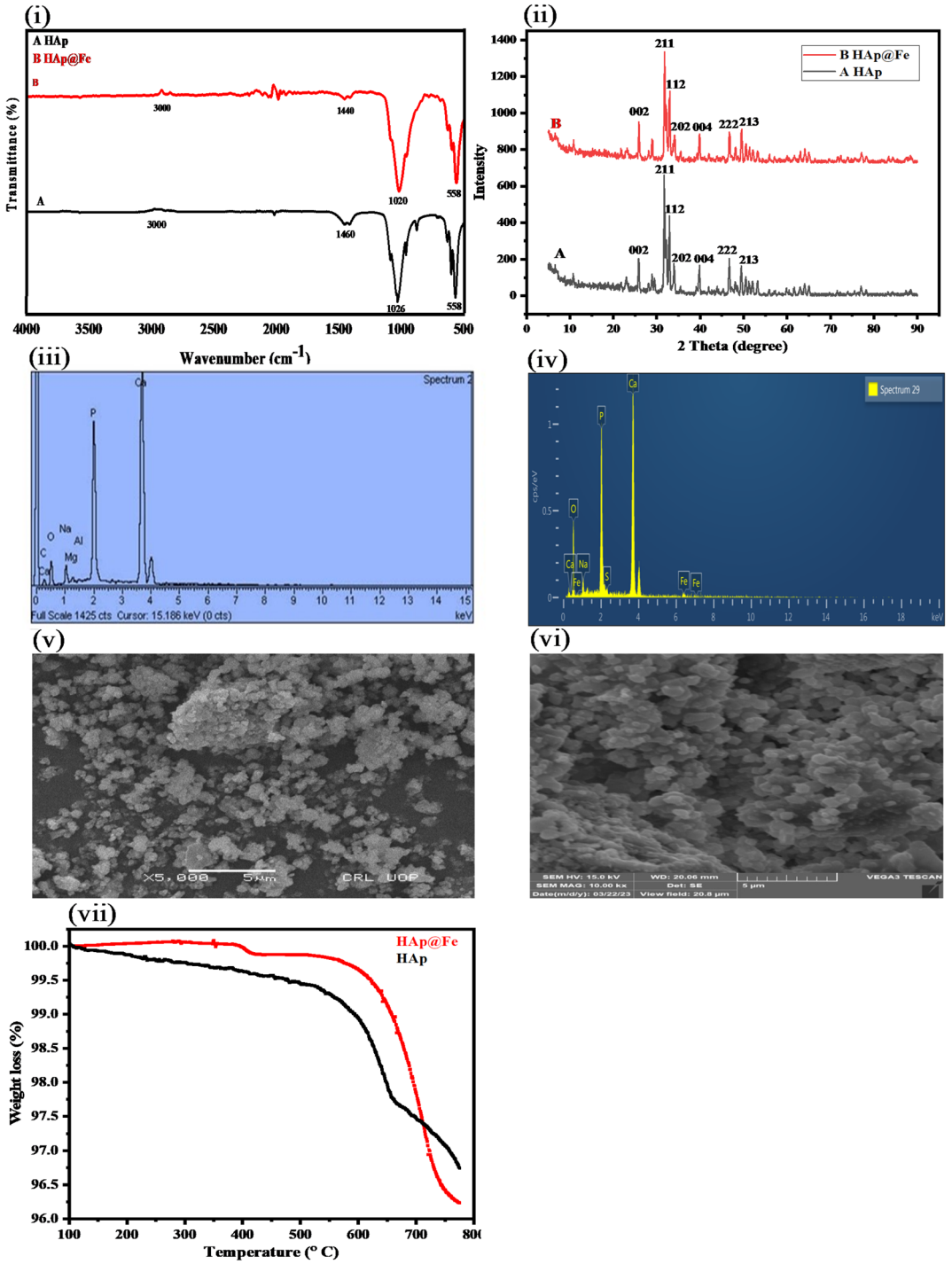

Fig. 1 (i) FTIR spectra of the prepared (A) HAp and (B) HAp@Fe_2O_3 indicate the presence of phosphate, carbonate, and hydroxyl groups. (ii) XRD spectra of the prepared (A) HAp and (B) HAp@Fe_2O_3. The HAp crystal lattice contracts due to the ion exchange of Ca^{2+} with Fe^{3+}, which facilitates the reduction of crystalline size. (iii) EDX analysis of the prepared Hap; and (iv) HAp@Fe_2O_3. The HAp spectrum displays the distinctive peaks of Ca, P, and O; on the other hand, the HAp@Fe_2O_3 spectrum displays the additional peak indicating the presence of Fe. Moreover, it demonstrates that when Fe is added to the HAp structure, the intensity of Ca decreases. SEM analysis spectra of prepared (v) HAp and (vi) HAp@Fe_2O_3 indicate its nanoporous structure, which is highly desirable for an expanded surface area. (Vii) TGA analysis of synthesized HAp and HAp@Fe_2O_3 indicates the high thermal stability of the synthesized platform.

because of its easy handling and the use of common instruments for the isolation of HAp.[13]

HAp and its nanocomposites have been used in various fields, such as diagnosis and overcoming environmental hazards.[14] These composites are efficient in the removal of dyes like Congo red, methylene blue, *etc.*[15] According to reports, HAp/chitosan nanocomposite is a promising option for tissue engineering, especially for scaffolds made of bone and cartilage.[16] Novel immunosensors have been reported using HAp nanocrystals, gold nanoparticles, and chitosan mixed thoroughly with anti-PSA antibodies for the diagnosis of prostate cancer.[17]

Various methods, such as ion-beam sputter coating[18] and electrophoretic deposition[19] are used for adding metal ions to HAp. In comparison to these methods, doping is more efficient because ionic doping can result in crystallinity of HAp, changes in thermal stability, grain size, lattice parameters, crystal structure phase decomposition, microstructure, and solubility depending on the amount and size of the dopant.[20]

In the current work, we synthesized HAp@Fe_2O_3 using the calcination method. The novelty of this work lies in the use of HAp@Fe_2O_3 for the sensing of ascorbic acid using chromogenic substrate (TMB) with the assistance of H_2O_2. In this process, the mimic enzyme (HAp@Fe_2O_3) provides a platform for the conversion of TMB into an oxidized form with the help of the oxidizing agent H_2O_2. Upon addition of AA, the oxidized form of TMB reversed back to its reduced (colorless) form, as observed with the naked eye and confirmed through a UV-Vis spectrophotometer. A new, fast, extremely sensitive, and selective AA detection method was developed. Different reaction conditions, such as HAp@Fe_2O_3 quantity, pH, TMB concentration, and incubation time, were optimized to get the best performance of the proposed platform. The proposed sensor was also applied to quantitatively check the concentration of ascorbic acid in physiological samples.

2 Experimental

2.1. Reagents-and-materials

All of the studies employed analytical-grade compounds; no additional purification was carried out. Double-distilled water was utilized to prepare the solutions. Ascorbic acid (≥97.0%), iron nitrate nonahydrate ($Fe(NO_3)_3 \cdot 9H_2O$), NaOH (≥97.0%), hydrogen chloride (98%), H_2O_2 (35%), and TMB were utilized. We acquired all of the chemicals from Sigma-Aldrich.

2.2. Instrumentation

Fourier transform infrared spectroscopy (FTIR) was used for the identification of the characteristic peaks of HAp@Fe_2O_3 in the range 4000–500 cm^{-1} (Agilent Technologies, Danbury, Conn, USA). The resolution of 4 cm^{-1} and 256 scans per sample were selected. A scanning electron microscope coupled to an energy dispersive X-ray spectrophotometer (SEM-EDS) with a TESCAN VEGA (LMU) SEM with INCAx-act (Oxford Instruments) was used to study the morphology and elemental composition of the synthesized platform. Phase identification of the prepared HAp@Fe_2O_3 was confirmed by X-ray diffraction (Shimadzu, LabX XRD-6100). The thermal stability was observed by thermogravimetric analysis of TGA (Pyris-1, V-3.81 PerkinElmer). A UV-Vis spectrophotometer was used for taking the absorption spectra (Shimadzu, UV, 1,800, Japan).

2.3. Synthesis of hydroxyapatite

Chicken waste bones were collected from a local restaurant. To remove any visible fleshy tissues adhering to bones, a thorough cleansing procedure was carried out. First of all, the bones were washed thoroughly with distilled water. Subsequently, the bones were crushed into small pieces and subjected to distilled water and acetone treatment. The meticulously cleaned waste bones were immersed in a 1 M NaOH solution. This was followed by proper washing and drying for 24 hours at 70 °C.[21] The extraction of inorganic HAp from the processed chicken bones was achieved through calcination at 800 °C. Pre-treated and dried bone pieces (10 g) were placed in alumina crucibles and subjected to calcinations in order to remove all the organic components. The temperature was gradually increased at a heating rate of 5 °C per minute and heated to 800 °C for a period of 8 hours.

Table 1 EDX analysis of HAp and HAp@Fe_2O_3

	HAp		HAp@Fe_2O_3	
Element	Weight (%)	Atomic (%)	Weight (%)	Atomic (%)
C	6.87	13.84	—	—
O	26.72	40.41	47.68	67.13
Na	3.70	3.89	2.59	2.54
Mg	0.57	0.57	—	—
Al	0.27	0.24	—	—
P	20.76	16.22	15.54	11.30
Ca	41.12	24.83	32.08	18.03
S	—	—	0.50	0.35
Fe	—	—	1.61	0.65
Total	100.00	100.00	100.00	100.00

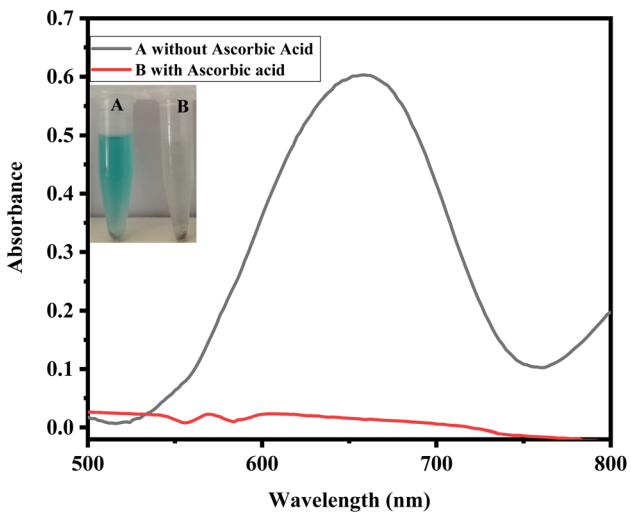

Fig. 2 UV-Vis spectra of the sensing reaction. The addition of 4 mg HAp@Fe_2O_3, 150 μL TMB (12 mM), 100 μL (24 mM) hydrogen peroxide, and 120 μL (A) without ascorbic acid and (B) with 150 μL ascorbic acid (56 μM).

2.4. Synthesis of iron doped HAp

The process involves treating iron nitrate nonahydrate ($Fe(NO_3)_3 \cdot 9H_2O$) with HA powder derived from broiler chicken bone in a ratio of 1 : 9 by weight. The resulting mixture of powdered substances was gradually heated and fused within high-alumina crucibles while being covered. This fusion was performed at a rate of 5 °C per minute and maintained for three hours at a temperature of 800 °C. Subsequently, the crucibles were allowed to cool down to room temperature.[22]

2.5. Detection of ascorbic acid

For the colorimetric detection of ascorbic acid, TMB was used as a chromogenic substrate in the presence of HAp@Fe_2O_3. The experiment was performed as follows: TMB underwent oxidation assisted by H_2O_2 in the presence of the synthesized platform. This resulted in a color change from colorless to blue-green. The protocol involves the mixing of 4 mg of HAp@Fe_2O_3, 500 μL of PBS buffer solution (6 mM), 200 μL of TMB (12 mM), and 100 μL of hydrogen peroxide (24 mM). Subsequently, 100 μL of ascorbic acid (0.6–56 μM) were added to the reaction mixture. This was followed by the incubation of the reaction mixture for 75 seconds. After the addition of ascorbic acid, the color changes from blue-green to colorless owing to the reduction of TMB. The anticipated change in visible range was also authenticated through a UV-Vis spectrophotometer.[23]

3 Results and discussions

3.1. Characterization result

3.1.1. FTIR analysis of HAp and HAp@Fe_2O_3. Fig. 1(i) shows the Fourier transform infrared spectroscopy of pure HAp and HAp@Fe_2O_3. The FTIR spectra indicate a lack of substantial disparity between the HAp and HAp@Fe_2O_3 materials. Each peak corresponds to a distinctive feature of HAp. The bands falling around 558 cm^{-1} and 1020 cm^{-1} correspond to the phosphate group present in the synthesized platform. Additionally, the peaks around 1440 cm^{-1}, represent the presence of the carbonate group, which remains in the structure from organic moieties despite pyrolysis at high temperatures.[24] The peaks above 3000 cm^{-1} represent the presence of OH group functionality in the proposed synthesized platform and HAp.[25]

3.1.2. X-ray diffraction (XRD) pattern of fabricated nanocomposite. The crystalline structure of both HAp and HAp@Fe_2O_3 was identified using the XRD patterns as shown in Fig. 1(ii). Diffraction peaks for HAp were visible at 2θ values of 26.12°, 31.14°, 32.16°, and 34.46°, respectively, which correspond to the (002), (211), (112), and (202) planes. Similarly, the 2θ values of 26.16° (002), 31.7° (211), 32.2° (112), and 34.72° (202), diffraction peaks of iron oxide HAp@Fe_2O_3 were found, confirming the formation of a crystallized hexagonal HAp@Fe_2O_3 structure. It is clear from the figure that the pristine form of HAp shows sharp peaks, whereas HAp@Fe_2O_3 shows slight broadening and comparatively less intense peaks. This broadening of the peaks can be attributed to the incorporation of Fe_2O_3 in the structure of HAp. It results in the generation of a slight amorphous phase within the crystalline structure of Hap.[26] This incorporation is performed strategically to achieve a balance between the crystallinity of the material and the amount of Fe_2O_3. The Scherrer equation was used to determine the crystal size of the prepared HAp and HAp@Fe_2O_3. The average crystalline size of HAp and HAp@Fe_2O_3 is 32.54 and 27.91 nm, respectively. This result indicates that the incorporation of Fe into HAp results in a reduction in crystallite size.[25]

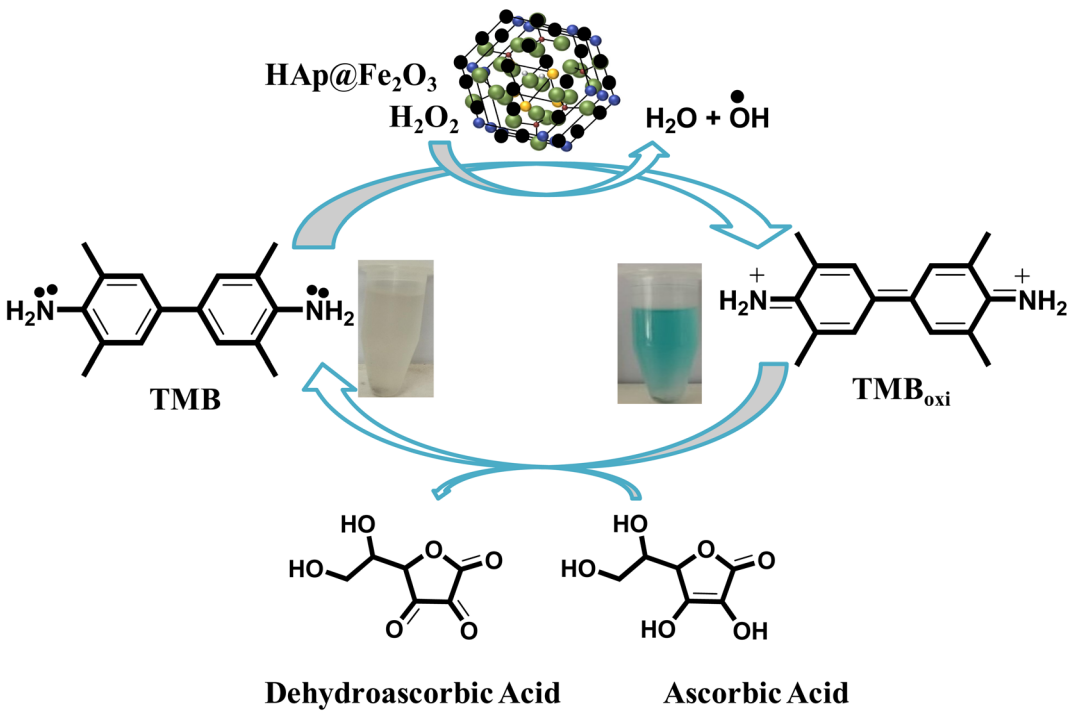

Scheme 1 Proposed mechanism for the sensing of ascorbic acid based on the HAp@Fe_2O_3 mimic enzyme assisted by H_2O_2.

3.1.3. EDX analysis of HAp and HAp@Fe_2O_3. Energy-dispersive X-ray (EDX) analysis was used to evaluate the elemental composition of HAp and HAp@Fe_2O_3. For the HAp specimen, the EDX investigation identified multiple elements[27] including carbon (6.87%), oxygen (26.72%), sodium (3.70%), magnesium (0.57%), aluminum (0.27%), phosphorus (20.76%), and calcium (41.12%) as shown in Table 1 and Fig. 1(iii). Similarly, for the HAp@Fe_2O_3 sample, the elemental composition was identified as phosphorus (15.54%), calcium (32.08%), oxygen (47.68%), sodium (2.59%), iron (1.61%), and sulfur (0.50%) by weight, as shown in Table 1 and Fig. 1(iv).

3.1.4. SEM analysis of the prepared HAp and HAp@Fe_2O_3. The SEM images of the synthesized HAp and HAp@Fe_2O_3 are shown in Fig. 1(v and vi). The morphology shows the nano-structure of the synthesized HAp and HAp@Fe_2O_3. This shows that the successful synthesis of the HAp (A) and HAp@Fe_2O_3 (B)

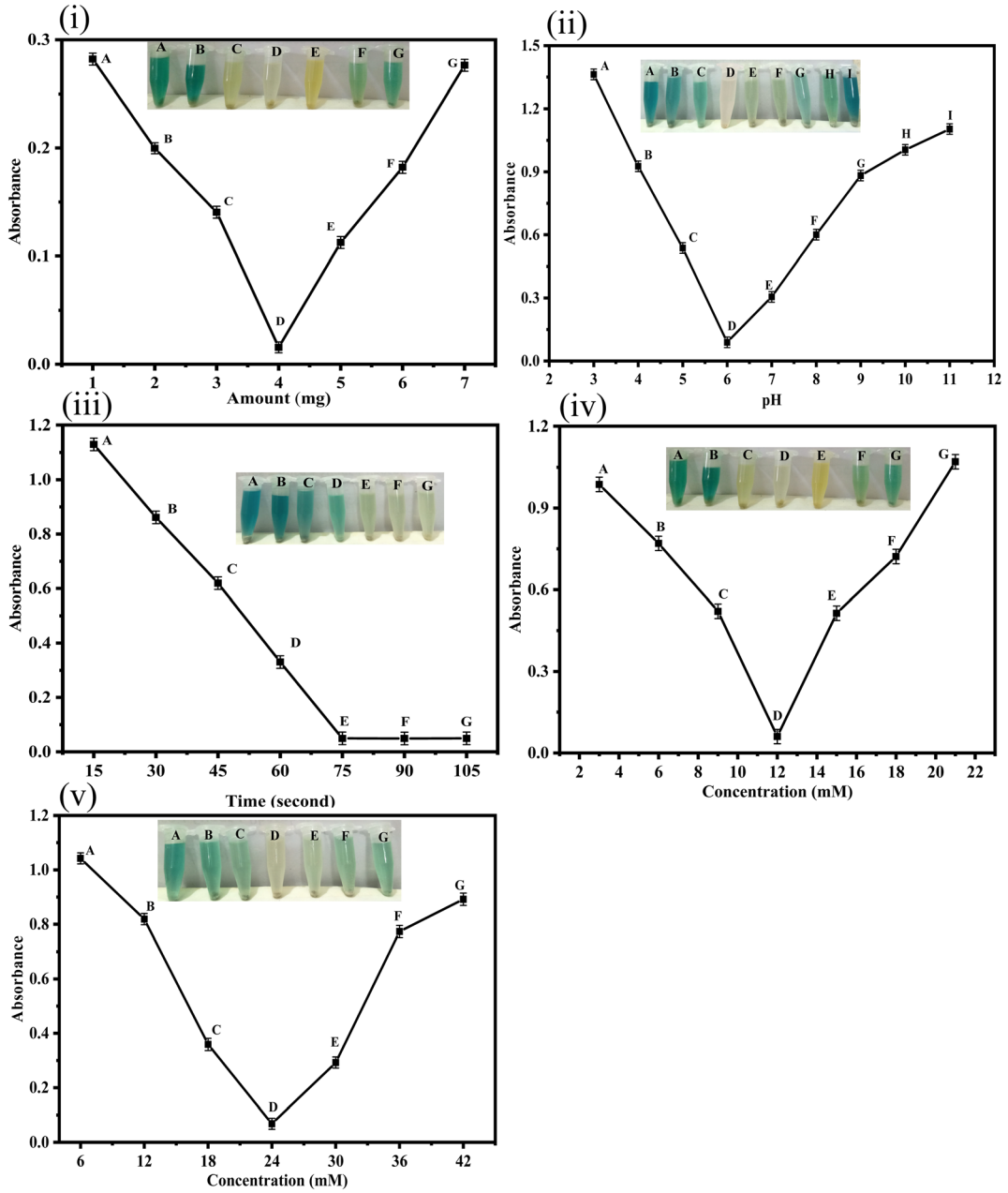

Fig. 3 (i) HAp@Fe_2O_3 was optimized at 1–7 mg. The best colorimetric response was observed at 4 mg HAp@Fe_2O_3. Conditions: 4 mg HAp@Fe_2O_3, 150 μL TMB (12 mM), 100 μL (24 mM) hydrogen peroxide, and 120 μL ascorbic acid (56 μM). (ii) AA, HAp@Fe_2O_3, and TMB solution interaction is demonstrated at different pH levels (3–9) in PBS at 4 mg HAp@Fe_2O_3 [ascorbic acid] = 56 μM (120 μL). The ideal colorimetric response was obtained at a pH of 6. (iii) Effect of time (15–105 seconds) at 4 mg HAp@Fe_2O_3, ascorbic acid 56 μM (150 μL). The reduction of TMB in the presence of ascorbic acid is very fast due to the high reducing power of AA. The color of the mixture changed from blue-green to transparent in a few seconds. (iv) Effect of TMB (2–20 mM) on the reaction oxidized by catalyst and H_2O_2 at 4 mg HAp@Fe_2O_3, ascorbic acid 56 μM (150 μL) were optimized, and the optimal concentration of TMB was found to be 12 mM. (v) The effect of H_2O_2 (6–42 mM) at 4 mg HAp@Fe_2O_3 [ascorbic acid] = 56 μM (150 μL) on the reaction was optimized, and the optimal response was shown at 24 mM.

nanoparticles having a structure with an expanded surface area is highly needed for the catalytic activity of our synthesized platform. By introducing iron into the HAp, we can further decrease the particle size, increase the surface area, and make it a better reactive surface for catalytic activities due to the enrichment of electrons. The structure of HAp, combined with its biocompatibility and osteoconductivity, the presence of both acidic and basic moieties, and the doping with Fe, make it an excellent surface for catalytic reactions.[28]

3.1.5. TGA analysis of HAp and HAp@Fe_2O_3. The TGA study of the synthesized HAp and HAp@Fe_2O_3 was carried out in order to find their thermal stability as shown in Fig. 1(vii). There is a steady decrease in the weight of the HAp with an increase in temperature after 250–700 °C, indicating the loss of organic material present in the sample. On the other hand, in HAp@Fe_2O_3, there is no decrease in weight up to around 650 °C, indicating the robustness and high thermal stability of our synthesized platform. A sudden, slight weight loss of up to 3% in HAp@Fe_2O_3 can be observed beyond 650 °C, indicating its high thermal stability. Beyond 700 °C, no visible weight loss was observed, as shown in the TGA curve.

3.2. Colorimetric determination of ascorbic acid

Fig. 2 shows the colorimetric detection of ascorbic acid. The following optimum experimental conditions were followed: HAp@Fe_2O_3 (4 mg) was mixed with 500 μL of PBS solution (6 mM) and 200 μL of TMB solution (12 mM), followed by the addition of 100 μL of hydrogen peroxide solution (24 mM) in an Eppendorf tube. This combination led to a color change from colorless to blue-green, which was observed with the naked eye. After the addition of ascorbic acid to 120 μL (56 μM), the blue-green color changed to a colorless form. Fig. 6 presents both the UV-Vis spectra and a visual colorimetric change.[29]

3.3. Proposed mechanism of the reaction

In the current work, the proposed sensor, HAp@Fe_2O_3, functions as a mimic enzyme. With the assistance of H_2O_2, the mimic enzyme converts the TMB into oxidized TMB, resulting in the formation of a blue-green color. Here, H_2O_2 helps in the generation of hydroxyl free radicals, which attack TMB and generate a colored complex. The generation of hydroxyl free radicals from H_2O_2 is catalyzed by the mimic enzyme. The addition of ascorbic acid to this complex results in the reduction of TMB, which becomes colorless in its reduced form. The oxidation of ascorbic acid results in the formation of dehydroascorbic acid. With the addition of ascorbic acid, the free radical generated from hydrogen peroxide by the catalytic action of HAp@Fe_2O_3 was scavenged. This scavenging of free radicals by ascorbic acid results in no oxidation of TMB. This colorimetric change was also confirmed with a UV-Vis spectrophotometer. The oxidized TMB showed maximum absorption at 652 nm (Scheme 1).

3.4. Optimization of various parameters

3.4.1. Effect of HAp@Fe_2O_3 amount. Fig. 3(i) shows the concentration optimization of the mimic enzyme (HAp@Fe_2O_3). For the optimization of HAp@Fe_2O_3, various concentrations of the platform (1–7 mg) were added to the reaction at optimized conditions. The best colorimetric response was observed at 4 mg. So the 4 mg of HAp@Fe_2O_3 was used for further experiments. The reaction was performed as follows: 4 mg of HAp@Fe_2O_3 was added to an Eppendorf tube along with 500 μL of phosphate-buffer solution (6 mM), 200 μL of TMB solution, 100 μL of H_2O_2, and 100 μL of ascorbic acid

Table 2 Comparsion of peroxidase like activity of HAp@Fe_2O_3 and HRP

Catalysts	Substrate	V_{max} (10^{-8} M s^{-1})	K_m (mM)	Reference
HRP	TMB	17.19	0.424	35
HRP	H_2O_2	10.55	3.240	
HAp@Fe_2O_3	TMB	15.4	3.11	This work
HAp@Fe_2O_3	H_2O_2	23.5	6.90	

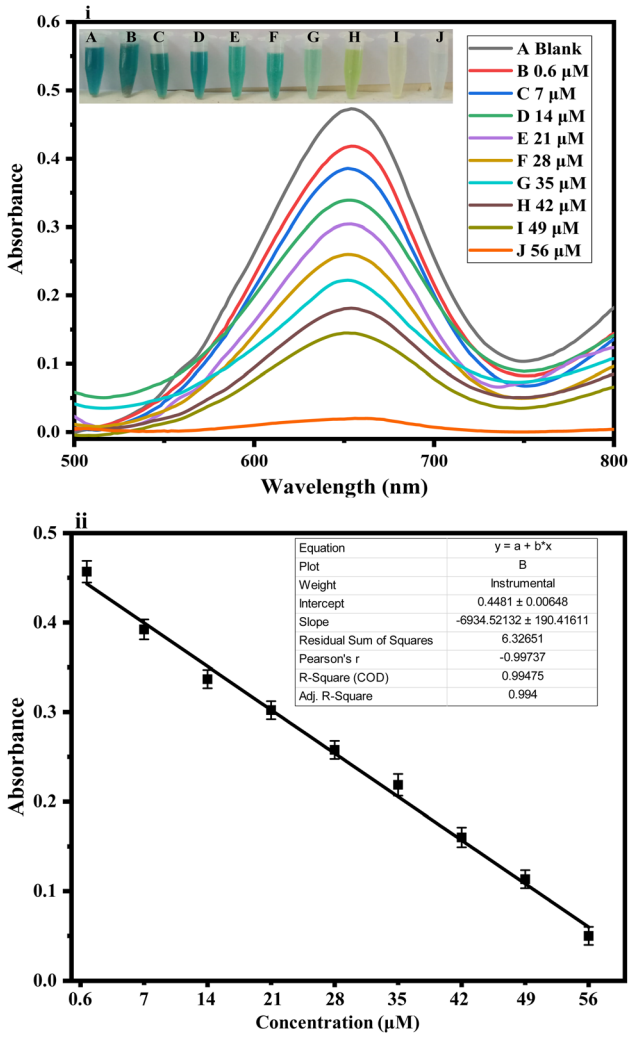

Fig. 4 HAp@Fe_2O_3-based AA biosensor (i) UV-Vis spectra and colorimetric change with respect to change in different concentrations (0.6–56 μM) of ascorbic acid. (ii) Calibration plot of AA concentrations *versus* absorbance conditions: 4 mg HAp@Fe_2O_3, 150 μL TMB (12 mM), 100 μL (24 mM) hydrogen peroxide, and 120 μL ascorbic acid (56 μM).

solution with a concentration of 56 μM. Upon the addition of ascorbic acid after 75 seconds, the color completely changed from blue-green to a colorless product in the presence of 4 mg HAp@Fe_2O_3. Deniz Uzunoğlu *et al.* reported that 100 μL of Fe NPs solution was optimum for the colorimetric detection of ascorbic acid.[30]

3.4.2. pH optimization. Fig. 3(ii) shows the optimization of pH for the proposed fabricated sensor. To efficiently control and adjust the response of the suggested sensor, various pH values ranging from 3 to 9 were examined. The best colorimetric response of the proposed biosensor was observed at pH 6. TMB's poor solubility in aqueous solutions—which is enhanced by the protonation of one of these substrates' amino groups—is the cause of its acid-dependent reactivity. Nevertheless, further pH reduction causes both amino groups to become protonated, rendering the substrate resistant to catalytic oxidation processes.[31] In the case of graphitic carbon nitride nanosheets, pH 4 was observed as the optimum pH for the sensing of chromium(VI) and ascorbic acid.[32]

3.4.3. Effect of time on sensitivity. Fig. 3(iii) shows the optimization of time for the proposed sensor. Ascorbic acid was colorimetrically detected in the presence of the peroxidase-like activity of HAp@Fe_2O_3. For the optimization of time, we performed the experiments at different time intervals of 15–105 seconds under optimized conditions. The best colorimetric response was observed at 75 seconds. The optimization of time was done at the optimum experimental conditions: 4 mg of HAp@Fe_2O_3, 500 μL of phosphate-buffer solution (6 mM), 200 μL of TMB solution, 100 μL of H_2O_2, and 100 μL of an ascorbic acid solution with a concentration of 56 μM. While Edwin *et al.* reported that 3 minutes is optimum for the colorimetric detection of ascorbic acid.[33]

3.4.4. Optimization of TMB concentration. Fig. 3(iv) shows the optimization of TMB concentration. The ability of HAp@Fe_2O_3 was evaluated using TMB as a substrate. Optimization of TMB concentration was done using various solutions of TMB in the range of 3–21 mM. 12 mM TMB concentration was observed to be optimal for the proposed sensor, as can be seen in the figure. The color changed from colorless to blue-green upon the addition of 4 mg HAp@Fe_2O_3, 150 μL TMB (12 mM), 100 μL (24 mM) hydrogen peroxide, and 120 μL Ascorbic Acid (56 μM). While in the reported literature 0.8 mM concentration, 15.4 μL TMB (52 mM concentration) was observed to be optimal for the proposed sensor.[34]

3.4.5. Optimization of H_2O_2. Fig. 3(v) shows the optimization of hydrogen peroxide. The preferred oxidizing agent for the

Table 3 Comparative analysis of proposed biosensor

S. no.	Materials used	Method applied	Linear range (μM)	LOD (μM)	References
1	CQDs	Colorimetric	1.0–105	0.14	36
2	Cu–Ag/rGO	Colorimetric	5–30	3.8	37
3	Papain-Ag NPs	Colorimetric	0.25–50	0.079	38
4	Pt/CeO_2 nanocomposites	Colorimetric	0.5–30	0.08	39
5	Smartphone based CD spectrometer	Colorimetric	0.6250–40	0.4946	40
6	Silica coated Au nanorods	Colorimetric	0.1–2.5	0.049	41
7	Graphene quantum dots	Colorimetric	0.3–10	0.094	42
8	M-CQDs	Colorimetric	10–70	3.26	43
9	HAp@Fe_2O_3	Colorimetric	0.6–56	0.16	Present work

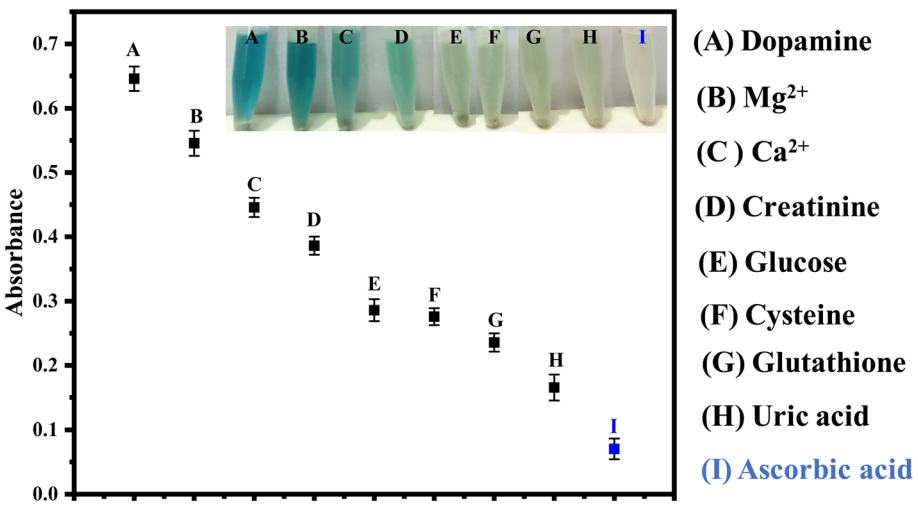

Fig. 5 Selectivity of the fabricated sensor was checked at optimized conditions (56 μM) for dopamine, Mg^{2+}, Ca^{2+}, glucose, uric acid, creatinine, and ascorbic acid. It can be seen that the TMB is completely reduced by AA at the optimized experimental conditions.

reporter TMB solution is H_2O_2. As a result, various H_2O_2 concentrations (6–42 mM) were used to achieve the optimum H_2O_2 concentration. The optimum (24 mM) H_2O_2 concentration was observed for the proposed sensor at optimum experimental conditions of 4 mg HAp@Fe_2O_3, 150 μL TMB (12 mM), 100 μL (24 mM) hydrogen peroxide, and 120 μL ascorbic acid (56 μM). While E. Davidson *et al.* reported that a (2 M) H_2O_2 concentration was optimum for the sensing of ascorbic acid.[33]

3.4.6. Peroxidase like activity of HAp@Fe_2O_3. The peroxidase-like activity of the mimic enzyme (HAp@Fe_2O_3) was analyzed using Michaelis–Menten kinetics. Catalysts with high values of V_{max} and lower values of K_m are desirable. The results of the current work and comparison with the reported literature are given in Table 2. It is clear from the results that the mimic enzyme shows comparable values of V_{max} when compared to horseradish peroxidase (HRP) for both substrates.

3.4.7. Effect of ascorbic acid concentration. The proposed biosensor was applied to measure the concentration of ascorbic acid. Fig. 4(i) shows the absorbance spectra of ascorbic acid by using various concentrations of AA in the range of 0.6–56 μM in an optimized condition. Utilizing the peroxidase mimic activity of HAp@Fe_2O_3 in the presence of TMB substrate, a sensitive approach was developed for the colorimetric detection of ascorbic acid under optimal experimental conditions. In the absence of ascorbic acid, a peak at 652 nm was observed by using a UV-Vis spectrophotometer. After the addition of ascorbic acid, the peaks gradually decreased by increasing the concentration of ascorbic acid. At a concentration of 56 μM of AA, the peak was completely reduced, and the color changed from blue-green to colorless. By using the calibration graph as shown in Fig. 4(ii), the proposed colorimetric sensor of ascorbic acid within a linear range of 0.6–56 μM with a limit of detection (LOD) of 0.16 μM and a LOQ of 0.53 μM were calculated using the formulas LOD (3*SD/slope) and LOQ (10*SD/slope). The limit of detection and linear range of the present study were compared with the reported literature, as shown in Table 3. It is clear from the table that the fabricated platform has exceptional sensitivity and a wide linear range.

3.5. Selectivity study of the proposed method

The selectivity of the proposed sensor, HAp@Fe_2O_3, is shown in Fig. 5. In the presence of commonly co-existing substances, including dopamine, uric acid, Mg^{2+}, glucose, creatinine, and Ca^{2+}, the selectivity of the proposed sensor was found to be excellent. The results illustrate that with the addition of ascorbic acid, the color completely changed from blue-green to colorless, while with the addition of dopamine, uric acid, Mg^{2+}, glucose, creatinine, and Ca^{2+}, no color change was observed. The proposed biosensor showed significant selectivity for the detection of ascorbic acid, as indicated in the results.

Under the aforementioned experimental conditions, the reproducibility of the proposed sensors was tested after each preparation. We observed a high level of reproducibility in the results. The response of the fabricated sensor was tested over a period of 6 months. For this purpose, periodically each month, the sensor response was evaluated. There was no considerable difference in the response of the sensor over the mentioned period of time. This highlighted the stability of the proposed sensing platform.

3.6. Application of the fabricated sensor

To examine the practical use of the fabricated platform, we employed the proposed sensor for detecting ascorbic acid in physiological solutions, as shown in Fig. 6(i). We applied the proposed sensor for the detection of ascorbic acid concentrations within the range of 0.6–56 μM in physiological solutions. Different concentrations of ascorbic acid in physiological solutions, such as 10, 18, and 33 μM, were prepared and introduced to the fabricated sensor. Using a UV-Vis spectrophotometer, we investigated the alteration in colorimetric

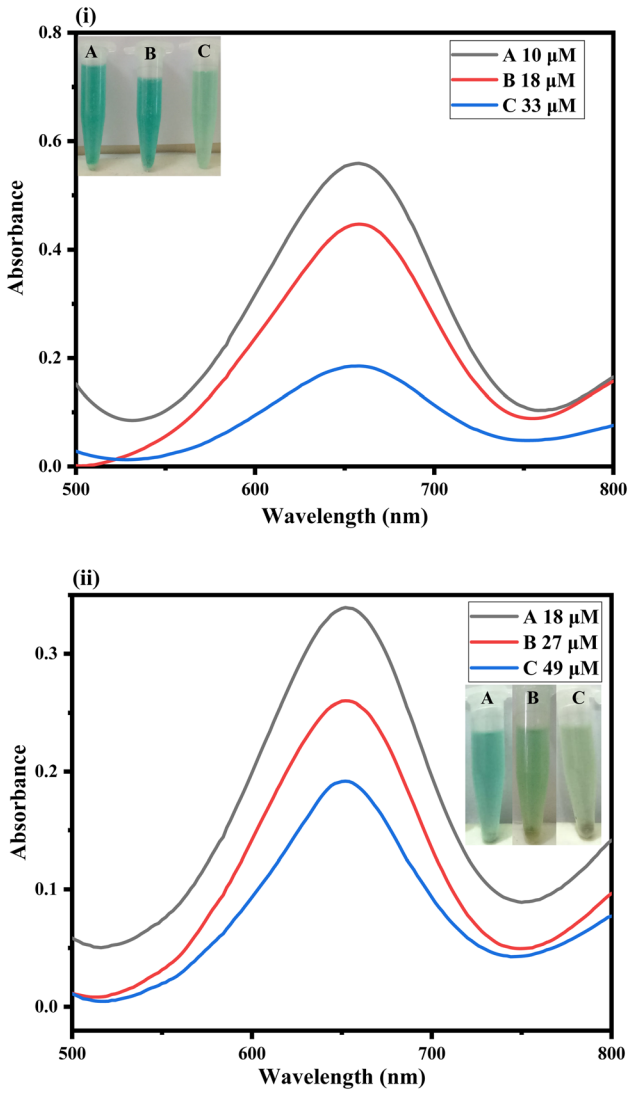

Fig. 6 (i) Physiological sample analysis spectra of the proposed sensor. Different concentrations of ascorbic acid in physiological solution at optimized conditions [4 mg HAp@Fe_2O_3, 150 μL TMB (12 mM), 100 μL (24 mM) hydrogen peroxide, and 120 μL ascorbic acid (56 μM)]. (ii) shows the colorimetric response of the proposed sensor and the corresponding UV-Vis spectra under optimized conditions for the sensing of ascorbic acid in real samples.

detection of ascorbic acid within physiological solutions. We observed an absorption peak at 652 nm that exhibited a linear decrease in absorbance with the rise in ascorbic acid concentration within the optimized time.[34] It proves that our suggested sensor is highly effective for detecting ascorbic acid in physiological solutions. Subsequently, blood plasma samples were collected from the Al-Habib clinical laboratory near the DHQ hospital in Kohat, KP, Pakistan. The samples were screened for the detection of ascorbic acid in the linear range of the proposed sensor. Strategic dilution of the real samples was performed to bring the analyte concentration into the linear range of our proposed sensor as and when needed. The response was observed with the naked eye and confirmed through a UV-Vis spectrophotometer, as shown in Fig. 6(ii).

4 Conclusion

In conclusion, a new, straight-forward, highly thermally stable, low-cost, biocompatible, highly sensitive, and selective sensing platform for ascorbic acid was fabricated. All the characterizations confirmed the successful synthesis of the mimic enzyme ($HAp@Fe_2O_3$). The fabricated sensor detected ascorbic acid with high sensitivity and selectivity in the presence of a bunch of potential interfering species. Comprehensive optimization studies were performed to fine-tune the sensing parameters, such as the amount of mimic enzyme (4 mg), pH (6), time (75 seconds), TMB concentration (12 mM), and H_2O_2 concentration (24 mM). The proposed sensor exhibited an extensive linear range of 0.6–56 μM, with a very low limit of detection (0.16 μM) and limit of quantification (0.53 μM) and an R^2 value of 0.998. These results indicate the fabricated platform is highly sensitive, and there is a strong correlation between absorption and concentration. The fabricated sensor was successfully used to detect ascorbic acid in physiological solutions. The sensing platform has the potential to be used for the diagnosis of diseases caused by the change in ascorbic acid. It can also be used in the food industry for the monitoring of different food samples.

Conflicts of interest

The authors declare that there is no conflict of interests.

Acknowledgements

Authors wish to thanks Researchers Supporting Project Number (RSP2024R45) at King Saud University Riyadh Saudi Arabia for financial support.

References

1 H. Guan, B. Han, D. Gong, Y. Song, B. Liu and N. Zhang, Colorimetric sensing for ascorbic acid based on peroxidase-like of GoldMag nanocomposites, *Spectrochim. Acta, Part A*, 2019, **222**, 117277.
2 C.-L. Sun, H.-H. Lee, J.-M. Yang and C.-C. Wu, The simultaneous electrochemical detection of ascorbic acid, dopamine, and uric acid using graphene/size-selected Pt nanocomposites, *Biosens. Bioelectron.*, 2011, **26**(8), 3450–3455.
3 Y. Matsuoka, M. Yamato and K.-i. Yamada, Fluorescence probe for the convenient and sensitive detection of ascorbic acid, *J. Clin. Biochem. Nutr.*, 2016, **58**(1), 16–22.
4 B. Chandrashekar and B. K. Swamy, Simultaneous cyclic voltammetric determination of norepinephrine, ascorbic acid and uric acid using TX-100 modified carbon paste electrode, *Anal. Methods*, 2012, **4**(3), 849–854.
5 U. Nishan, S. Rehman, R. Ullah, A. Bari, S. Afridi, M. Shah, J. Iqbal, M. Asad, A. Badshah and N. Khan, Fabrication of a colorimetric sensor using acetic acid-capped drug-mediated copper oxide nanoparticles for nitrite biosensing in processed food, *Front. Mater.*, 2023, **10**, 1169945.
6 M. Asad, N. Muhammad, N. Khan, M. Shah, M. Khan, M. Khan, A. Badshah, Z. Latif and U. Nishan, Colorimetric acetone sensor based on ionic liquid functionalized drug-mediated silver nanostructures, *J. Pharm. Biomed. Anal.*, 2022, **221**, 115043.
7 B. X. V??ng and T. H. J. M. Linh, The Extraction of pure hydroxyapatite from porcine bone by thermal process, *Metall. Mater. Eng.*, 2019, **25**(1), 47–58.
8 N. Muhammad, Y. Gao, F. Iqbal, P. Ahmad, R. Ge, U. Nishan, A. Rahim, G. Gonfa and Z. Ullah, Extraction of biocompatible hydroxyapatite from fish scales using novel approach of ionic liquid pretreatment, *Sep. Purif. Technol.*, 2016, **161**, 129–135.
9 N. M. Pu'ad, P. Koshy, H. Abdullah, M. Idris and T. Lee, Syntheses of hydroxyapatite from natural sources, *Heliyon*, 2019, **5**(5), e01588.
10 T. McGauran, N. Dunne, B. M. Smyth and E. Cunningham, Feasibility of the use of poultry waste as polymer additives and implications for energy, cost and carbon, *J. Cleaner Prod.*, 2021, **291**, 125948.
11 M. V. Khvostov, M. S. Borisova, N. V. Bulina, S. V. Makarova, N. B. Dumchenko, T. G. Tolstikova and N. Z. Lyakhov, The influence of zinc and silicate ions on biological properties of hydroxyapatite synthesized by a mechanochemical method, *Ceram. Int.*, 2021, **47**(7), 9495–9503.
12 K. W. Goh, Y. H. Wong, S. Ramesh, H. Chandran, S. Krishnasamy, A. Sidhu and W. Teng, Effect of pH on the properties of eggshell-derived hydroxyapatite bioceramic synthesized by wet chemical method assisted by microwave irradiation, *Ceram. Int.*, 2021, **47**(7), 8879–8887.
13 R. A. Ramli, R. Adnan, M. A. Bakar and S. a. M. Masudi, Synthesis and characterisation of pure nanoporous hydroxyapatite, *J. Phys. Sci.*, 2011, **22**(1), 20–37.
14 S. Pai, M. S. Kini and R. Selvaraj, A review on adsorptive removal of dyes from wastewater by hydroxyapatite nanocomposites, *Environ. Sci. Pollut. Res.*, 2021, **28**, 11835–11849.
15 D. C. Manatunga, R. M. de Silva, K. Nalin de Silva, N. de Silva and E. Premalal, Metal and polymer-mediated synthesis of porous crystalline hydroxyapatite nanocomposites for environmental remediation, *R. Soc. Open Sci.*, 2018, **5**(1), 171557.

16 M. Nikpour, S. Rabiee and M. Jahanshahi, Synthesis and characterization of hydroxyapatite/chitosan nanocomposite materials for medical engineering applications, *Composites, Part B*, 2012, **43**(4), 1881–1886.

17 G. Shen, C. Cai and J. Yang, Fabrication of an electrochemical immunosensor based on a gold–hydroxyapatite nanocomposite–chitosan film, *Electrochim. Acta*, 2011, **56**(24), 8272–8277.

18 I. Pana, A. C. Parau, C. M. Cotrut, M. Dinu, D. M. Vranceanu, A. E. Kiss, G. Serratore, D. A. Böhner, C. Vitelaru and G. Ambrogio, Influence of deposition temperature on the structure and functional properties of Mg doped hydroxyapatite coatings deposited on manufactured AZ31B alloy substrates by RF magnetron sputtering, *Ceram. Int.*, 2023, **49**(13), 22340–22354.

19 L.-Y. Li, L.-Y. Cui, B. Liu, R.-C. Zeng, X.-B. Chen, S.-Q. Li, Z.-L. Wang and E.-H. Han, Corrosion resistance of glucose-induced hydrothermal calcium phosphate coating on pure magnesium, *Appl. Surf. Sci.*, 2019, **465**, 1066–1077.

20 I. Ratha, P. Datta, V. K. Balla, S. K. Nandi and B. Kundu, Effect of doping in hydroxyapatite as coating material on biomedical implants by plasma spraying method: A review, *Ceram. Int.*, 2021, **47**(4), 4426–4445.

21 E. Barua, A. B. Deoghare, P. Deb, S. D. Lala and S. J. M. T. P. Chatterjee, Effect of pre-treatment and calcination process on micro-structural and physico-chemical properties of hydroxyapatite derived from chicken bone bio-waste, *Mater. Today: Proc.*, 2019, **15**, 188–198.

22 N. T. Weissmueller, H. A. Schiffter, A. J. Pollard and A. C. J. M. L. Tas, Molten salt synthesis of potassium-containing hydroxyapatite microparticles used as protein substrate, *Mater. Lett.*, 2014, **128**, 421–424.

23 J. Peng, J. Ling, X.-Q. Zhang, L.-Y. Zhang, Q.-E. Cao, Z.-T. J. S. Ding and A. B. Chemical, A rapid, sensitive and selective colorimetric method for detection of ascorbic acid, *Sens. Actuators, B*, 2015, **221**, 708–716.

24 H. Sahana, D. K. Khajuria, R. Razdan, D. R. Mahapatra, M. Bhat, S. Suresh, R. R. Rao and L. Mariappan, Improvement in bone properties by using risedronate adsorbed hydroxyapatite novel nanoparticle based formulation in a rat model of osteoporosis, *J. Biomed. Nanotechnol.*, 2013, **9**(2), 193–201.

25 E. R. Kramer, A. M. Morey, M. Staruch, S. L. Suib, M. Jain, J. I. Budnick and M. J. J. O. M. S. Wei, Synthesis and characterization of iron-substituted hydroxyapatite via a simple ion-exchange procedure, *J. Mater. Sci.*, 2013, **48**, 665–673.

26 A. Khaliq, R. Nazir, M. Khan, A. Rahim, M. Asad, M. Shah, M. Khan, R. Ullah, E. A. Ali and A. Khan, Co-doped CeO_2/activated C nanocomposite functionalized with ionic liquid for colorimetric biosensing of H2O2 via peroxidase mimicking, *Molecules*, 2023, **28**(8), 3325.

27 U. Nishan, I. Ullah, N. Muhammad, S. Afridi, M. Asad, S. U. Haq, M. Khan, M. Soylak and A. J. A. J. f. S. Rahim, Engineering, Investigation of Silver-Doped Iron Oxide Nanostructures Functionalized with Ionic Liquid for Colorimetric Sensing of Hydrogen Peroxide, *Arabian J. Sci. Eng.*, 2023, **48**(6), 7703–7712.

28 M. Khalid, S. S. B. Jikan, S. Adzila, Z. Murni, N. Badarulzaman, R. Rosley and M. U. J. B. R. A. C. Hameed, Synthesis and characterizations of hydroxyapatite using precursor extracted from chicken egg shell waste, *Biointerface Res. Appl. Chem.*, 2022, **12**(4), 5663–5671.

29 U. Nishan, W. Ullah, N. Muhammad, M. Asad, S. Afridi, M. Khan, M. Shah, N. Khan and A. J. A. o. Rahim, Development of a nonenzymatic colorimetric sensor for the detection of uric acid based on ionic liquid-mediated nickel nanostructures, *ACS Omega*, 2022, **7**(30), 26983–26991.

30 D. Uzunoğlu and A. Özer, Facile Synthesis of Magnetic Iron-Based Nanoparticles from the Leach Solution of Hyperaccumulator Plant Pinus brutia for the Antibacterial Activity and Colorimetric Detection of Ascorbic Acid, *ACS Appl. Bio Mater.*, 2022, **5**(11), 5465–5476.

31 M. Drozd, M. Pietrzak, P. G. Parzuchowski, E. J. A. Malinowska and B. Chemistry, Pitfalls and capabilities of various hydrogen donors in evaluation of peroxidase-like activity of gold nanoparticles, *Anal. Bioanal. Chem.*, 2016, **408**, 8505–8513.

32 M. Rong, L. Lin, X. Song, Y. Wang, Y. Zhong, J. Yan, Y. Feng, X. Zeng and X. J. B. Chen, Bioelectronics, Fluorescence sensing of chromium (VI) and ascorbic acid using graphitic carbon nitride nanosheets as a fluorescent "switch", *Biosens. Bioelectron.*, 2015, **68**, 210–217.

33 E. Davidson, Z. Xi, Z. Gao and X. Xia, Ultrafast and sensitive colorimetric detection of ascorbic acid with Pd-Pt core-shell nanostructure as peroxidase mimic, *Sens. Int.*, 2020, **1**, 100031.

34 U. Nishan, U. Sabba, A. Rahim, M. Asad, M. Shah, A. Iqbal, J. Iqbal and N. J. M. C. Muhammad, Physics, Ionic liquid tuned titanium dioxide nanostructures as an efficient colorimetric sensing platform for dopamine detection, *Mater. Chem. Phys.*, 2021, **262**, 124289.

35 W. Xue, T. Cheng-Ling, L. Jia-Jun, H.-Z. ZHANG and W. Jian, Ultra-small CuS nanoparticles as peroxidase mimetics for sensitive and colorimetric detection of uric acid in human serum, *Chin. J. Anal. Chem.*, 2018, **46**(5), e1825–e1831.

36 X. Shu, Y. Chang, H. Wen, X. Yao and Y. Wang, Colorimetric determination of ascorbic acid based on carbon quantum dots as peroxidase mimetic enzyme, *RSC Adv.*, 2020, **10**(25), 14953–14957.

37 G. Darabdhara, B. Sharma, M. R. Das, R. Boukherroub and S. Szunerits, Cu-Ag bimetallic nanoparticles on reduced graphene oxide nanosheets as peroxidase mimic for glucose and ascorbic acid detection, *Sens. Actuators, B*, 2017, **238**, 842–851.

38 J. Peng, J. Ling, X.-Q. Zhang, L.-Y. Zhang, Q.-E. Cao and Z.-T. Ding, A rapid, sensitive and selective colorimetric method for detection of ascorbic acid, *Sens. Actuators, B*, 2015, **221**, 708–716.

39 X. Liu, X. Wang, C. Qi, Q. Han, W. Xiao, S. Cai, C. Wang and R. Yang, Sensitive colorimetric detection of ascorbic acid

using Pt/CeO_2 nanocomposites as peroxidase mimics, *Appl. Surf. Sci.*, 2019, **479**, 532–539.

40 L. Kong, Y. Gan, T. Liang, L. Zhong, Y. Pan, D. Kirsanov, A. Legin, H. Wan and P. Wang, A novel smartphone-based CD-spectrometer for high sensitive and cost-effective colorimetric detection of ascorbic acid, *Anal. Chim. Acta*, 2020, **1093**, 150–159.

41 G. Wang, Z. Chen and L. Chen, Mesoporous silica-coated gold nanorods: towards sensitive colorimetric sensing of ascorbic acid via target-induced silver overcoating, *Nanoscale*, 2011, **3**(4), 1756–1759.

42 J.-J. Liu, Z.-T. Chen, D.-S. Tang, Y.-B. Wang, L.-T. Kang and J.-N. Yao, Graphene quantum dots-based fluorescent probe for turn-on sensing of ascorbic acid, *Sens. Actuators, B*, 2015, **212**, 214–219.

43 S. Chandra, V. K. Singh, P. K. Yadav, D. Bano, V. Kumar, V. K. Pandey, M. Talat and S. H. Hasan, Mustard seeds derived fluorescent carbon quantum dots and their peroxidase-like activity for colorimetric detection of H_2O_2 and ascorbic acid in a real sample, *Anal. Chim. Acta*, 2019, **1054**, 145–156.